Intraparticle Convection Effect on Pressurization and Blowdown of Adsorbers

Z. P. Lu, J. M. Loureiro, M. D. LeVan, and A. E. Rodrigues
Laboratory of Separation and Reaction Engineering, School of Engineering, University of Porto, 4099 Porto Codex, Portugal

Pressurization and blowdown steps in pressure swing adsorption (PSA) with binary mixtures of inert and adsorbable species are studied. Modeling involves mass balances for the bulk fluid phase and inside particles, that is, intraparticle diffusion/convection models, momentum balance equations, and linear adsorption equilibrium isotherm. The importance of intraparticle convection in PSA is assessed. Mass transfer inside pores is enhanced by intraparticle convection, which leads to a better efficiency of adsorption (pressurization) and desorption (blowdown) processes. Performance is improved by intraparticle convection and lies between diffusion and equilibrium limits, as shown in propagation profiles of the adsorbable species mole fraction in the bed and inside particles.

Introduction

Pressure swing adsorption (PSA) has come a long way since it was invented by Skarstrom (1959). A major area of recent interest in PSA is the use of very rapid cycling, that is, a short pressurization (less than 1 second with large pressure drop) and a quite long exhaust (5-20 seconds), which results in a higher sorbent productivity at equal purity and recovery. It has been commercialized for the production of oxygen for medical purposes (Jones et al., 1980; Jones and Keller, 1981). The theoretical understanding of these new processes is primitive. In general, a PSA process is composed of pressurization, production (feed), blowdown and purge steps. A number of theoretical and experimental works on cases similar to feed (adsorption) and purge (desorption) steps (in which the pressure drop is negligible) have been published, but studies on the pressurization and blowdown steps are scarce.

Preliminary theoretical and experimental studies on pressurization and blowdown were carried out (Richter et al., 1982; Fernandez and Kenney, 1983; Sundaram and Wankat, 1988; Hart et al., 1990; Rodrigues et al., 1991b), and large effects of pressure drop on pressurization and blowdown steps in PSA cycles were found and discussed. Theoretical results of Doong and Yang (1988) also show strong effects of pressure drop on the separation performance of PSA and pressure swing parametric pumping processes.

The effect of pressure drop along the bed is more important when the cycle time decreases. In previous works (Sundaram and Wankat, 1988; Buzanowski et al., 1989; Hart et al., 1990; Rodrigues et al. 1991b), the local equilibrium assumption was considered, since very small adsorbent particles (around 0.02 cm in diameter) have been used in rapid PSA to minimize the mass-transfer resistance inside the adsorbent. No criteria are available to predict the conditions in which the mass-transfer resistance inside the absorbent is important in a PSA process. Such conditions can be found by a comparison of the results calculated from the equilibrium model and those from a model that considers mass-transfer resistance inside the absorbent. Mass-transfer resistance was empirically found to be important below a threshold value around 100 for the parameter $4D_e\tau_c/d_p^2$ (where τ_c is the cycle time) for a wide range of all the other parameters (Yang, 1987). This criterion was supported by experimental data on activated carbon for a number of binary mixtures (Yang and Doong, 1985; Yang et al., 1985). When lumping the information on all steps of a PSA process, this criterion appears to be very rough, since the time required normally differs for each step in a PSA process, and the superficial velocity at the open side of the bed in pressurization and blowdown steps is so high (particularly for a rapid PSA unit) that mass-transfer resistances inside the absorbent cannot be neglected. Anyway, very small adsorbent particles will cause unfavorable effects in desorption (Lu et al., 1991a) and increase the cycle time which is very important parameter in rapid PSA.

Correspondence concerning this article should be addressed to A. E. Rodrigues.
M. D. LeVan is presently at the Deparment of Chemical Engineering, University of Virginia, Charlottesville, VA 22903.

Usually, a pellet (zeolitic adsorbent) can be visualized as an ensemble of crystals with a microporous structure bound by a continuous macroporous medium. In micropores mass transfer occurs mainly by Knudsen and surface diffusion, while in macropores it occurs by diffusion (molecular and Knudsen) and convection (Rodrigues et al., 1982, 1991a, 1992). Based on the analysis of Ruckenstein et al. (1971), a semi-empirical criterion was suggested by Ruthven and Loughlin (1972) for the relative importance of the micropore and macropore mass transfer from the magnitude for the parameter:

$$\Omega = \frac{w(1-\epsilon_p)(D_c/d_c^2)}{\epsilon_p(D_p/d_p^2)}\left(\frac{dq}{dc_c}\right) \tag{1}$$

where w is the weight fraction of crystals in the pellet, dq/dc_c is the slope of the isotherm. They concluded that macropore control is more likely at relatively low temperatures, while at higher temperatures micropore resistance is probably the controlling step. It was suggested that if the Ω value is significantly less than 1, micropore resistance dominates; if $\Omega > 100$, macropore resistance controls. It should be noted that D_p is the "apparent" effective diffusivity in the macropores, since Ruthven and Loughlin (1972) did not consider the effect of convective, forced flow in macropores when they derived this relation.

If the mass-transfer resistance is not in the micropores, how can we reduce the mass-transfer resistance without reducing the particle size? A good choice will be the use of an absorbent containing "large-pores" (Rodrigues et al., 1991a, 1992; Lu et al., 1991a). Since the pressure drop is very large across the pellets in the open side of the bed in the pressurization and blowdown steps, particularly in a rapid PSA (Sundaram and Wankat, 1988; Hart et al., 1990; Rodrigues et al., 1991b), the intraparticle forced flow would largely improve the mass transfer inside the absorbent.

Recently, several experimental studies and theoretical models considering mass-transfer resistances inside the absorbent (pore diffusion and linear driving force) have been published (Cheng and Hill, 1985; Yang and Doong, 1985; Doong and Yang, 1986; Hassan et al., 1986, 1987; Shin and Knaebel, 1987, 1988; Farooq et al., 1989; Farooq and Ruthven, 1991). They focused primarily on the theoretical model and the effect of a few parameters on the performance of PSA (purity and recovery of the products), and assumed that pressure drop was negligible along the bed.

In this article, we focus on the dynamics of pressurization and blowdown of an isothermal bed by using three different models: intraparticle diffusion and convection, intraparticle diffusion, and equilibrium (Lu et al., 1991a). Our objective is to assess the differences in the propagation profiles of total pressure, velocity and mole fraction in the bed and inside the absorbent. Linear adsorption equilibrium isotherms are also considered, since their performance is good in a PSA cycle.

Mathematical Models

The dynamics of pressurization and blowdown of a bed have been studied by Sundaram and Wankat (1988), Hart et al., (1990), Rodrigues et al., (1991b), among others, assuming local equilibrium and Darcy's law for fluid flow. Zhong et al., (1992) used a nonisothermal model and accounted for intraparticle resistances (macropore + micropore); however, their analysis was limited to the case of a pure component (inert or adsorbable). The system considered here is an isothermal bed packed with "large-pore" adsorbent materials (slab geometry), and the feed is a binary mixture of species A (adsorbable) and B (inert). Intraparticle mass-transfer resistances are assumed to be due to diffusion and convection in the macropores; therefore, micropore resistance is considered to be negligible, as it is the case in many adsorption systems (Ruthven, 1992). Initially the bed is at steady state with a uniform mole fraction y_o of adsorbable species A at a pressure $P = P_l$ for pressurization and $P = P_h$ for blowdown. At time $t = 0$, a positive (for pressurization) or a negative (for blowdown) step change on total pressure is made at the bed inlet. The adsorption equilibrium isotherm is: $q_A = mc'_A$. Model equations in dimensionless form for the three models considered are given below using the following variables:

$$x = \frac{z}{L},\ \rho = \frac{z'}{\ell},\ f = \frac{c}{c_o} = \frac{P}{P_o},\ f' = \frac{c'}{c_o} = \frac{P'}{P_o},\ u^* = \frac{u}{u_o},\ v^* = \frac{v}{v_o},\ \theta = \frac{t}{\tau_o}$$

where

$c_o = \dfrac{P_o}{RT}$ = total concentration at atmospheric pressure,

$v_o = \dfrac{B_p}{\mu}\dfrac{\Delta P_o}{L}$ = reference intraparticle velocity,

$\tau_o = \dfrac{\epsilon L}{u_o}$ = reference space time

u_o = bulk fluid superficial velocity at the bed inlet in steady state at a given pressure drop $\Delta P_o = P_h - P_l$ (here $P_l = P_o$), that is,

$$u_o = \frac{-La_1/P_h + \sqrt{(La_1/P_h)^2 + 2La_2(1-(P_l/P_h)^2)}}{2La_2} \tag{2}$$

with

$$a_1 = \frac{150\mu(1-\epsilon)^2}{d_p^2\epsilon^3};\quad a_2 = \frac{1.75\rho_o(1-\epsilon)}{P_o d_p \epsilon^3} \tag{2a}$$

Case A: intraparticle diffusion + convection model

Mass balances inside the absorbent particle are:

$$\frac{\partial}{\partial\rho}\left(\frac{f'}{b_4+f'}\frac{\partial y'_A}{\partial\rho} + \frac{y'_A}{b_4}\frac{\partial f'}{\partial\rho}\right) - \lambda_o\frac{\partial(v^* f' y'_A)}{\partial\rho} = \alpha_o(1+\epsilon_p)\frac{\partial(f' y'_A)}{\partial\theta} \tag{3}$$

$$\frac{\partial}{\partial\rho}\left(\frac{1}{b_4}\frac{\partial f'}{\partial\rho}\right) - \lambda_o\frac{\partial(v^* f')}{\partial\rho} = \alpha_o\left[\frac{\partial f'}{\partial\theta} + \xi_p\frac{\partial(f' y'_A)}{\partial\theta}\right] \tag{4}$$

where $\xi_p = [(1-\epsilon_p)/\epsilon_p]m$ is the adsorbent capacity parameter. The boundary conditions are:

$$\rho = 0,\ y'_A = y_A - \frac{\partial y_A}{\partial x}\beta_R;\ f' = f - \frac{\partial f}{\partial x}\beta_R \tag{5}$$

$$\rho=1,\ y_A'=y_A+\frac{\partial y_A}{\partial x}\beta_R;\ f'=f+\frac{\partial f}{\partial x}\beta_R \tag{6}$$

and initial condition:

$$\theta=0,\ y_A'=y_o;\ f'=f_o;\ \forall x,\ \rho \tag{7}$$

where $f_o=f_\ell$ for the pressurization and $f_o=f_h$ for the blowdown.

Momentum equation for the fluid inside particle:

$$v^*=\frac{v}{v_o}=-\beta_\ell\frac{\partial f'}{\partial\rho} \tag{8}$$

Mass balances for the bulk fluid phase in a bed volume element are:
Species A:

$$\frac{\partial}{\partial x}\left(\frac{u^*f}{Pe}\frac{\partial y_A}{\partial x}\right)-\frac{\partial(u^*fy_A)}{\partial x}=\frac{\partial(fy_A)}{\partial\theta}+\frac{1-\epsilon}{\epsilon}N_A \tag{9}$$

Overall:

$$\frac{\partial(u^*f)}{\partial x}+\frac{\partial f}{\partial\theta}+\frac{1-\epsilon}{\epsilon}N=0 \tag{10}$$

where dimensionless fluxes of species A and overall are given by:

$$N_A=\frac{\epsilon_p}{\alpha_o}\left[\left(-\frac{f'}{b_4+f'}\frac{\partial y_A'}{\partial\rho}-\frac{y_A'}{b_4}\frac{\partial f'}{\partial\rho}+\lambda_o v^* f' y_A'\right)\Bigg|_{\rho=0}-\left(-\frac{f'}{b_4+f'}\frac{\partial y_A'}{\partial\rho}-\frac{y_A'}{b_4}\frac{\partial f'}{\partial\rho}+\lambda_o v^* f' y_A'\right)\Bigg|_{\rho=1}\right] \tag{11}$$

$$N=\frac{\epsilon_p}{\alpha_o}\left[\left(-\frac{1}{b_4}\frac{\partial f'}{\partial\rho}+\lambda_o v^* f'\right)\Bigg|_{\rho=0}-\left(-\frac{1}{b_4}\frac{\partial f'}{\partial\rho}+\lambda_o v^* f'\right)\Bigg|_{\rho=1}\right] \tag{12}$$

Momentum equation for the bulk fluid is:

$$-\frac{\partial f}{\partial x}=b_5u^*+b_6f(u^*)^2 \tag{13}$$

Ergun's equation is strictly valid for quasi-stable flows. Here, it is used locally in the bed as an approximation (Bird et al., 1960).

Boundary conditions associated with Eqs. 9 and 10 are:
Pressurization:

$$x=0,\ y_A-\frac{1}{Pe}\frac{\partial y_A}{\partial x}=y_f;\ f=f_h \tag{14}$$

$$x=1,\ \frac{\partial y_A}{\partial x}=0;\ \frac{\partial f}{\partial x}=0 \tag{15}$$

Blowdown:

$$x=0,\ \frac{\partial y_A}{\partial x}=0;\ f=f_\ell \tag{16}$$

$$x=1,\ \frac{\partial y_A}{\partial x}=0;\ \frac{\partial f}{\partial x}=0 \tag{17}$$

The initial condition associated with Eqs. 9 and 10 is:

$$\theta=0,\ y_A=y_o;\ f=f_o;\ \forall x,\ 0<x\le 1 \tag{18}$$

where $f_o=f_\ell$ for the pressurization and $f_o=f_h$ for the blowdown.

The definitions of the parameters, β_R, β_ℓ, b_1, b_2, b_3, b_4, b_5, b_6, Pe, λ, λ_o, α, α_o, and Φ can be found in Table 1.

Case B: intraparticle diffusion model

In the absence of intraparticle convection, $\lambda_o=0$; therefore, the intraparticle diffusion + convection model (case A) reduces to the intraparticle diffusion model.

Case C: equilibrium model

If there no mass-transfer resistances inside the particle, the intraparticle diffusion model reduces to the equilibrium model.

Model equations are (Rodrigues et al., 1991b):

In the bulk fluid phase:

$$\frac{\partial}{\partial x}\left(\frac{u^*f}{Pe}\frac{\partial y_A}{\partial x}\right)-\frac{\partial(u^*fy_A)}{\partial x}=\left[1+\epsilon_p\frac{1-\epsilon}{\epsilon}(1+\xi_p)\right]\frac{\partial(fy_A)}{\partial\theta} \tag{19}$$

$$-\frac{\partial(u^*f)}{\partial x}=\frac{\partial f}{\partial\theta}+\epsilon_p\frac{1-\epsilon}{\epsilon}\left[\frac{\partial f}{\partial\theta}+\xi_p\frac{\partial(fy_A)}{\partial\theta}\right] \tag{20}$$

Boundary and initial conditions are given by Eqs. 14–18.

Table 1. Definition of the Parameters

$b_1=\frac{\epsilon\gamma_1 D_{mo}}{Lu_o}$	$\frac{1}{\mathrm{Pe}}=\frac{\epsilon D_{ax}}{Lu}=\frac{b_1}{u^*f}+b_2$
$b_2=\frac{\epsilon\gamma_2 d_p}{L}$	$\lambda=\lambda_o v^*(b_4+f')$
$b_3=\frac{1}{\lambda_o}$	$\lambda_o=\frac{\tau_f\ell^2}{D_{mo}}\frac{v_o}{\epsilon_p\ell}$
$b_4=\frac{D_{mo}}{D_{kA}}$	$\alpha=\alpha_o u^*(b_4+f')$
$b_5=\frac{a_1L}{P_o}u_o$	$\alpha_o=\frac{\tau_f\ell^2}{D_{mo}}\frac{u_o}{\epsilon L}$
$b_6=a_2Lu_o^2$	$\beta_R=\frac{\ell}{2L}$
$\Phi=\frac{P_\ell}{P_h}$	$\beta_\ell=\frac{L}{\ell}\frac{P_o}{\Delta P_o}$
$\xi_p=\frac{1-\epsilon_p}{\epsilon_p}m$	

Table 2. Values of Fluid, Particle and System Properties Used in Numerical Simulations

$D_{mo}=0.1\ cm^2\cdot s^{-1}$	$\epsilon=0.4$
$\rho_o=10^{-3}g\cdot cm^{-3}$	$\epsilon_p=0.7$
$\mu=10^{-4}g\cdot cm^{-1}\cdot s^{-1}$	$L=150$ cm
$m=20$ and 100	$d_p=0.1$ and 0.03 cm
$P_l=P_o=100$ kPa	$\gamma_1=20$
$P_h=500$ and 2,000 kPa	$\gamma_2=0.5$
$\tau_f=4.5$	

Simulation Results and Discussion

The method of orthogonal collocation in finite elements is very useful for solving partial differential equations (Leitão and Rodrigues, 1990; Rodrigues et al., 1991b; Lu et al., 1991a,b). The commercial PDECOL package was used to solve the equations for the three models. Details can be found elsewhere (Lu et al., 1991a). The calculation was stopped when $|f_h-f_{(x=1)}|/f_l < 1\%$ for the pressurization and $|f_l-f_{(x=1)}|/f_l < 1\%$ for the blowdown.

The numerical simulations presented here are restricted to the pressurization and blowdown steps. The pressurization step was studied using an input of high-pressure gas of a binary mixture (inert and adsorbable species) with $y_f=0.5$, which is equal to the uniform initial concentration y_o in the bed. The blowdown was started with an uniform initial $y_o = 0.5$ concentration in the bed. The effects of the adsorbent size $d_p=0.03$ and 0.1 cm, adsorbent capacity measured by the slope of the linear isotherm $m = 20$ and 100, and pressure ratio $\Phi = P_l/P_h=0.2$ and 0.05 are addressed. Values of fluid, particle and system properties are listed in Table 2.

Effect of the particle size d_p

The resistances to mass transfer inside the particles can be reduced by decreasing the particle size. However, very small particles imply large pressure drops in the bed which, in turn, impose severe limitations to the mechanical design of the absorbent and absorber. On the other hand, smaller particles correspond to longer pressurization and blowdown times: the smaller the particle size, the larger the cycle time of a PSA process, which is an important parameter of the process productivity.

The pressurization times with two different particle sizes ($d_p = 0.1$ and 0.03 cm) are compared in Figure 1a, where the history of reduced total pressure f at the closed end of the bed ($x=1$) is represented. For smaller particles the bed takes more than double the time to be completely pressurized, mainly because for smaller particles the fluid flow in the bed is in the laminar regime most of the time, whereas for larger particles

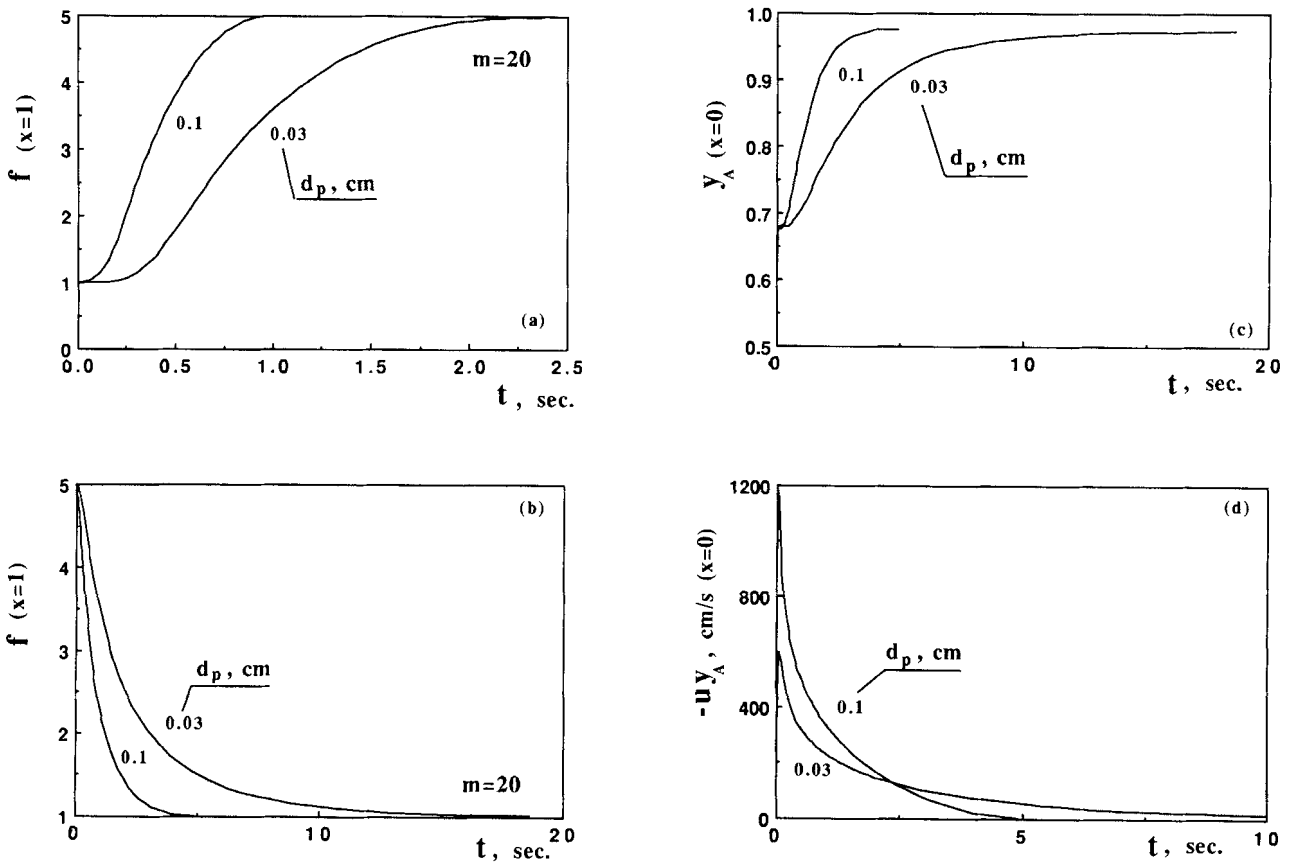

Figure 1. Equilibrium model solution (case C) with two particle sizes ($d_p=0.1$ and 0.03 cm): $\Phi=0.2$, $m=20$.

(a) History of reduced total pressure f at the closed end ($x=1$) during pressurization; (b) History of reduced total pressure f at the closed end ($x=1$) during blowdown; (c) History of adsorbable species mole fraction y_A at the bed outlet ($x=0$) during blowdown; (d) History of adsorbable species mole flux ($-uy_A$) at the bed outlet ($x=0$) during blowdown.

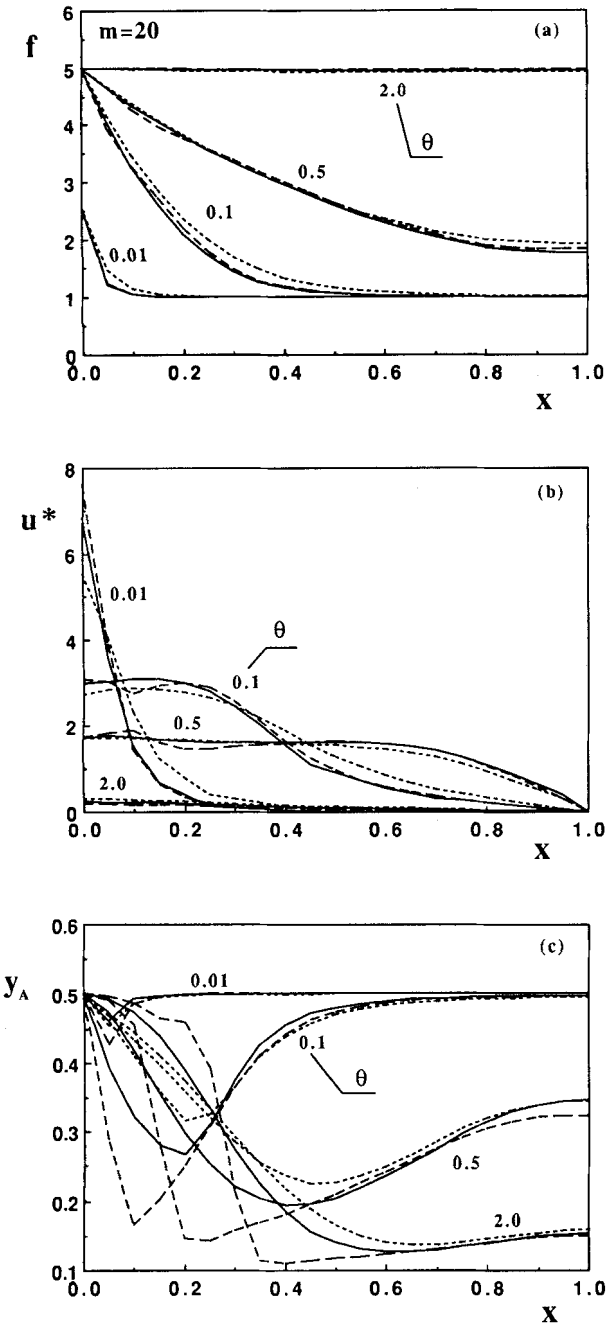

Figure 2. Axial profiles of (a) reduced total pressure *f*, (b) reduced velocity u^*, and (c) mole fraction y_A during pressurization.

$\Phi = 0.2$, $m = 20$, $d_p = 0.1$ cm, $u_o = 135$ cm/s, $\tau_o = 0.446$ s; —— case A ($B_p = 1.25 \times 10^{-9}$ cm^2), ····· case B, ------ case C.

the turbulent regime near the open end is maintained for longer times. The implication of the flow regime on the pressurization time was already shown by Rodrigues et al., (1991c) using either Ergun's or Darcy's laws as the momentum equations. The difference is even clearer during the blowdown, as can be seen from Figure 1b. Nevertheless, as the Peclet numbers are very high in both situations, the final concentation profiles of the adsorbable component are expected to be very similar for both particle sizes (Rodrigues et al., 1991b,c).

The histories of mole fraction and mole flux of adsorbable species at the open end ($x = 0$) during the blowdown for both adsorbent sizes are shown in Figures 1c and 1d, respectively. The simulations in these figures correspond to the equilibrium model (case C) with the parameter values $m = 20$, $\Phi = 0.2$, and $d_p = 0.03$ and 0.1 cm; other parameters are listed in Table 2. These figures show that the smaller particle size corresponds not only to a lower productivity of the adsorbent due to the increase in the pressurization and blowdown times, but also to lower purity and recovery of the products, since the adsorbable species is more difficult to desorb due to high pressures in the bed (Lu et al., 1991a); as a consequence, more of this species will remain in the column at the end of blowdown. The above conclusions are to be taken carefully since they apply only when the resistances inside the particle are negligible; when the intraparticle resistance is the controlling step, it can be useful to decrease this resistance by reducing the particle size.

The question arises about the possibility of enhancing the mass transfer inside the adsorbent without decreasing the particle size. Figure 2a shows that during the pressurization large pressure gradients exist near the open end of the bed, exactly where the majority of the mass transfer between fluid and solid occurs; the same is true during the blowdown (Rodrigues et al., 1991b,c). The mass transfer inside the absorbent can then be enhanced if large-pore materials are used, since a convective flow develops inside the particles (Rodrigues et al., 1982, 1991a).

The conclusion that using bigger particles with large pores can lead to a better bed design that using smaller particles for the same column performance, pressure drop and adsorbent productivity can also be drawn by extending the scaling rules introduced by Wankat and his coworkers (Wankat, 1987; Wankat and Koo, 1988; Rota and Wankat, 1990). As an example, let us consider macropore diffusion as the controlling step and an "old" configuration with $d_p = 0.1$ cm, $L = 100$ cm, and $D = 100$ cm. If adsorbent productivity needs to be four times higher for the same separation performance by reducing the particle size to $d_p = 0.05$ cm, then the "new" configuration would be a short, fat column with $L = 25$ cm and $D = 100$ cm (laminar flow) and a column with $L = 31.5$ cm and $D = 89$ cm (turbulent flow). Practical problems with packing, flow distribution, and end effects should be very carefully accounted for in the design of the new column. However, if a large-pore adsorbent with the same "old" d_p is used, the new configuration would have $L = 50$ cm and $D = 70.7$ cm (for laminar flow) and $L = 40$ cm and $D = 80$ cm (for turbulent flow), with the requirement that $\lambda = 24$ in the "new" configuration.

In pressurization and blowdown steps where intraparticle Peclet number λ changes with time and position, the required λ can be the average value. For both new configurations described previously, the blowdown times ($m = 20$, $\Phi = 0.2$) multiplied by four (to account for the intensification procedure) are 22% higher than those for old configurations when using the smaller particle size and 11% lower when using the same particle size with large pores.

Intraparticle diffusion/convection and equilibrium models

The equilibrium model is a limiting case corresponding to

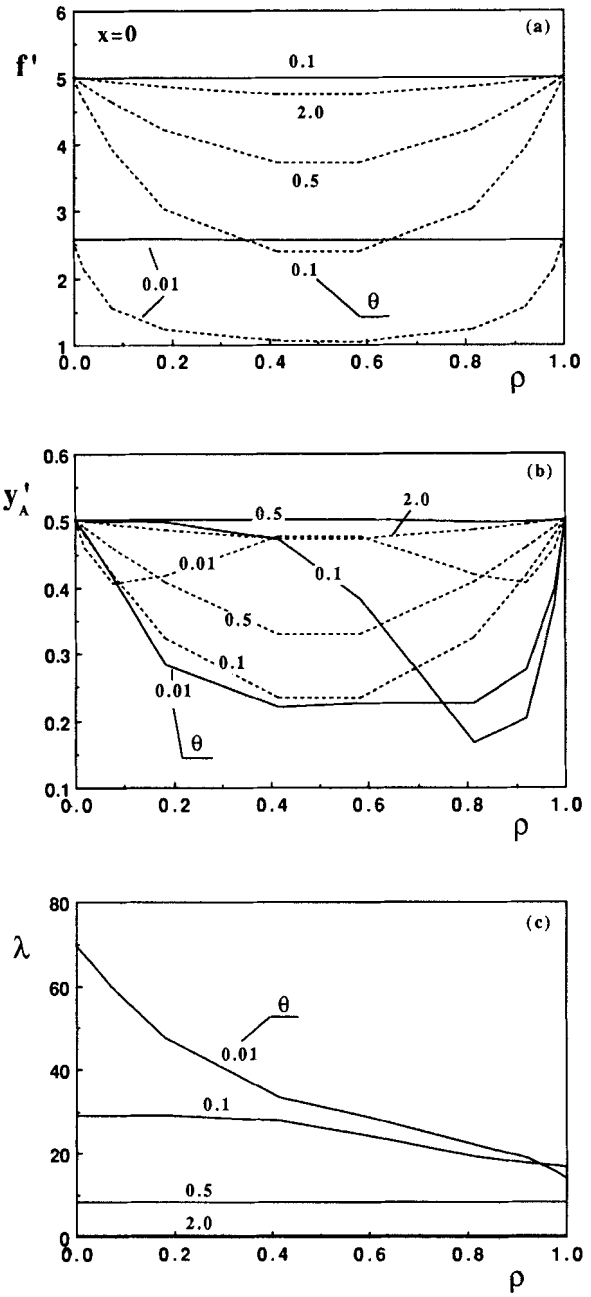

Figure 3. Intraparticle profiles of (a) reduced total pressure f', (b) mole fraction y'_A, and (c) intraparticle Peclet number λ, at the bed inlet ($x=0$) during pressurization.

$\Phi=0.2$, $m=20$, $d_p=0.1$ cm, $u_o=135$ cm/s, $\tau_o=0.446$ s; —— case A ($B_p=1.25\times10^{-9}$ cm^2), ····· case B.

the absence of mass-transfer resistances; when intraparticle resistances are present, the diffusion model is normally used to simulate the behavior of the system. If large pressure gradients exist along the bed, with large-pore materials, a convective flow develops inside the particles which is superimposed to the diffusive flow, enhancing the mass-transfer relative to diffusion alone. Intraparticle convection then improves the bed dynamics between the limits corresponding to diffusion-and equilibrium-controlled situations.

Pressurization. In Figures 2a-2c, the axial profiles of reduced pressure f, reduced velocity u^*, and mole fraction y_A are shown at different times during pressurization as calculated by the three models: diffusion + convection (case A, solid lines), diffusion (case B, dotted lines), and equilibrium (case C, dashed lines). The values of the parameters used in the simulations were $m=20$, $\Phi=0.2$, $d_p=0.1$ cm, $u_o=135$ cm/s, $\tau_o=0.446s$, and $B_p=1.25\times10^{-9}$ cm^2 (case A). Since there is a mass-transport limitation between fluid and adsorbent, the pressure in the bed increases faster in case B than in case C at the beginning of pressurization. Finally, it takes a little longer to reach the pressure plateau in the bed for case B, since the adsorbent is not saturated yet, even at the end of pressurization: at $|f_{(x=1)}-f_h|/f_f<1\%$, the adsorbent may be incompletely saturated at the local partial pressure in each position.

There is a crossing point between the pressure profiles for cases B and C, whose axial position varies with time during pressurization. The same is true for the axial velocity profiles. This is so because, near the open end at short times during pressurization, larger velocities are observed with the equilibrium model due to the absence of mass-transfer resistances (adsorption causes larger local pressure gradients); at longer times, on the other hand, as in the absence of mass-transfer resistances the adsorbent is already saturated near this open end, the reverse is true.

As expected, the more dispersive mole fraction profiles are obtained in case B (diffusion model); it is not surprising then that the penetration length is larger (the pressurization amount is smaller) in case B than in case C (the equilibrium model) (Rodrigues et al., 1991b,c; Lu et al., 1991b). Also, the dispersive nature of the concentration propagation in case B results in an earlier breakthrough in the following step, the feed (production) step in a PSA process. As the figures show, case A (diffusion + convection) is located between these two extrema (cases B and C); moreover, it is expected that case A approaches case C when the particle permeability B_p is increased (Lu et al., 1991a).

Let us now consider in greater detail how the intraparticle convection enhances the mass transfer inside the particles.

We know already (Rodrigues *et al.*, 1991a) that the mass transfer inside particles depends on one parameter α (ratio between the local diffusion time constant and the local space time) when the diffusion model is considered, whereas it depends on two parameters α and λ (local intraparticle Peclet number) when intraparticle convection and diffusion are taken into account. Both α and λ vary with position and time due to pressure and velocity variations.

For the same simulations shown in Figures 2a–2c, the profiles of reduced pressure f' and mole fraction y'_A inside the particles for case A (solid lines) and case B (dotted lines) are shown in Figures 3a, 3b, 4a and 4b at the axial positions $x=0$ and $x=0.25$, respectively. In the absence of intraparticle convection ($\lambda=0$, case B), the profiles are always symmetric around the center of the particle. Since α is much smaller at $x=0.25$ than at $x=0$, the profiles at $x=0.25$ are smoother. At the end of pressurization, $|f_{(x=1)}-f_h|/f_f<1\%$, the profiles do not reach the plateaus corresponding to the particle skin total pressure and mole fraction which means that the adsorbent is not yet saturated at the local partial pressure.

The situation is different when intraparticle convection is present (case A). The axial profiles of reduced total pressure

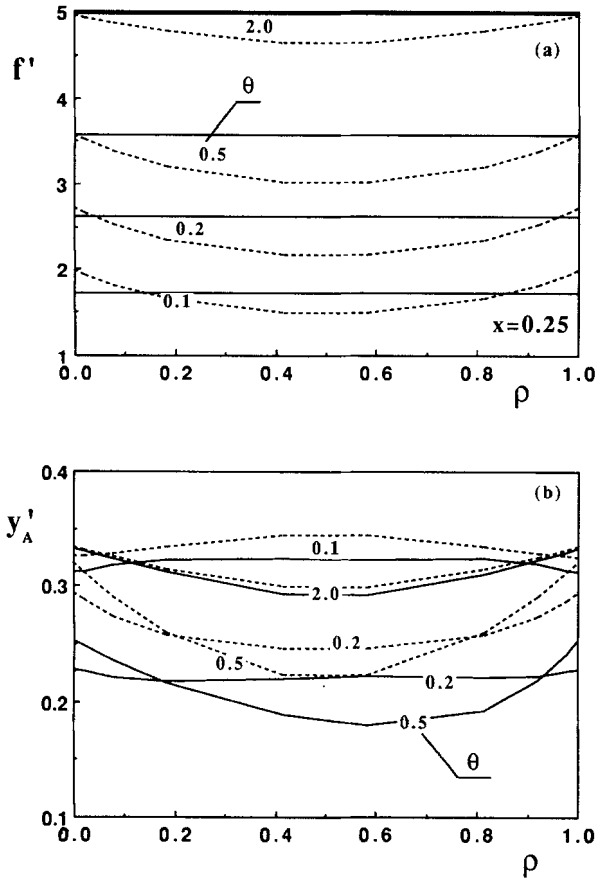

Figure 4. Intraparticle profiles (a) reduced total pressure f' and (b) mole fraction y'_A at the axial position $x = 0.25$ in the bed during pressurization.

$\Phi = 0.2$, $m = 20$, $d_p = 0.1$ cm, $u_o = 135$ cm/s, $\tau_o = 0.446$ s; —— case A ($B_p = 1.25 \times 10^{-9}$ cm^2), ····· case B.

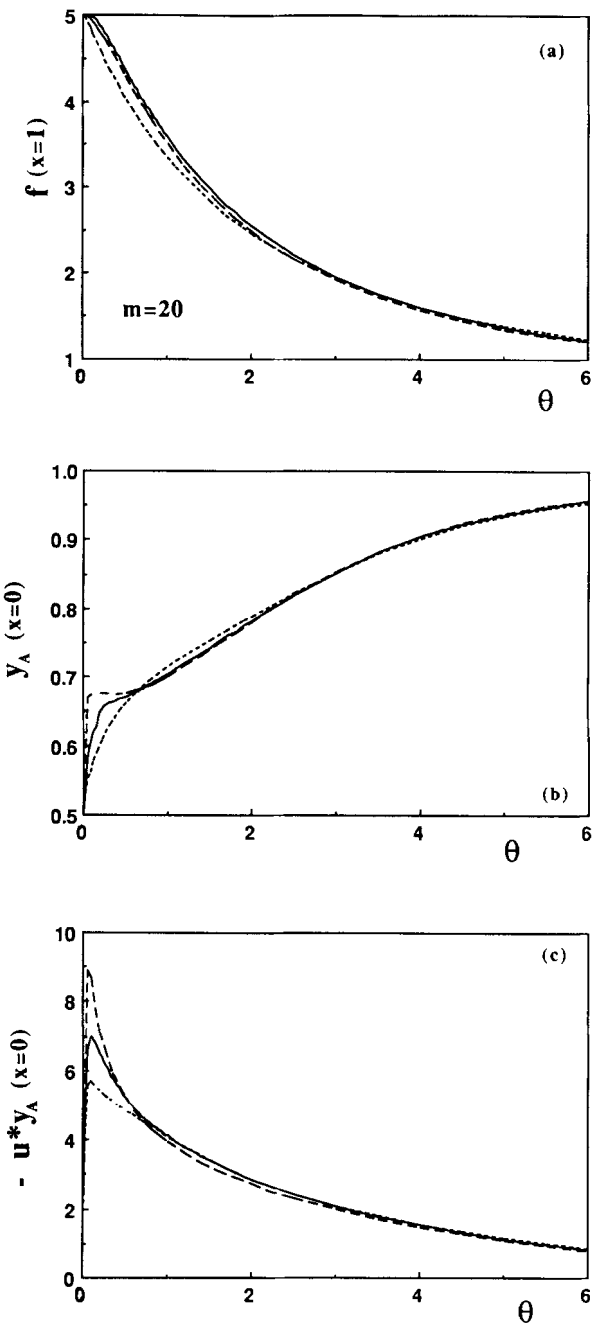

Figure 5. Histories of (a) reduced total pressure f at the closed end ($x = 1$), (b) mole fraction y_A, and (c) mole flux ($-u^* y_A$) at the open end ($x = 0$) during blowdown.

$\Phi = 0.2$, $m = 20$, $d_p = 0.1$ cm, $u_o = 135$ cm/s, $\tau_o = 0.446$ s; —— case A ($B_p = 1.25 \times 10^{-9}$ cm^2), ····· case B, ------- case C.

keep a plane shape at almost all times, and the mole fraction profiles are not symmetric around the particle center; moreover, near the open end of the bed, the local saturation plateau of the adsorbent is reached (Figure 3b) due to the mass transfer by convection. The profile of the intraparticle Peclet number λ at several times at the axial position $x = 0$ is shown in Figure 3c; high intraparticle Peclet numbers are observed at short times (with very low pressure gradients inside the particles, Figure 3a), increasing the local intraparticle mass transfer. At $x = 0.25$, since the pressure drop in the bed is small (relative to the one at $x = 0$), the intraparticle convective flow is small, and again, the local saturation plateau is not reached at the end of pressurization (Figure 4b). The effect of the intraparticle convection decreases as we move away from the open end of the column.

The relative importance of the convective flow through the particle can be assessed from Figures 3a-3c. It can be concluded that the intraparticle convective velocity at $x = 0$ is only about 0.24% of the superficial velocity through the bed at $\theta = 0.01$, decreasing to about 0.01% at $\theta = 2$. However, if a comparison is made between the fluxes through the particles with and without convection, it can be shown that the intraparticle molar flux of species A with convection, at $\theta = 0.01$, is 4.44 times the flux without convection. The intraparticle convective flux contributes 82.6% of the total molar flux of A. At $\theta = 0.1$ the intraparticle molar flux of A when convection is present is 3.44 times higher than the corresponding flux in the absence of convection. The contribution of the intraparticle convection at $\theta = 0.1$ accounts for 48.4% of the intraparticle molar flux of species A. The relative importance of the intraparticle convective flux decreases with time, becoming negligible at $\theta \geq 0.5$; in fact, at $x = 0$, most of the mass transfer occurs before $\theta = 0.5$.

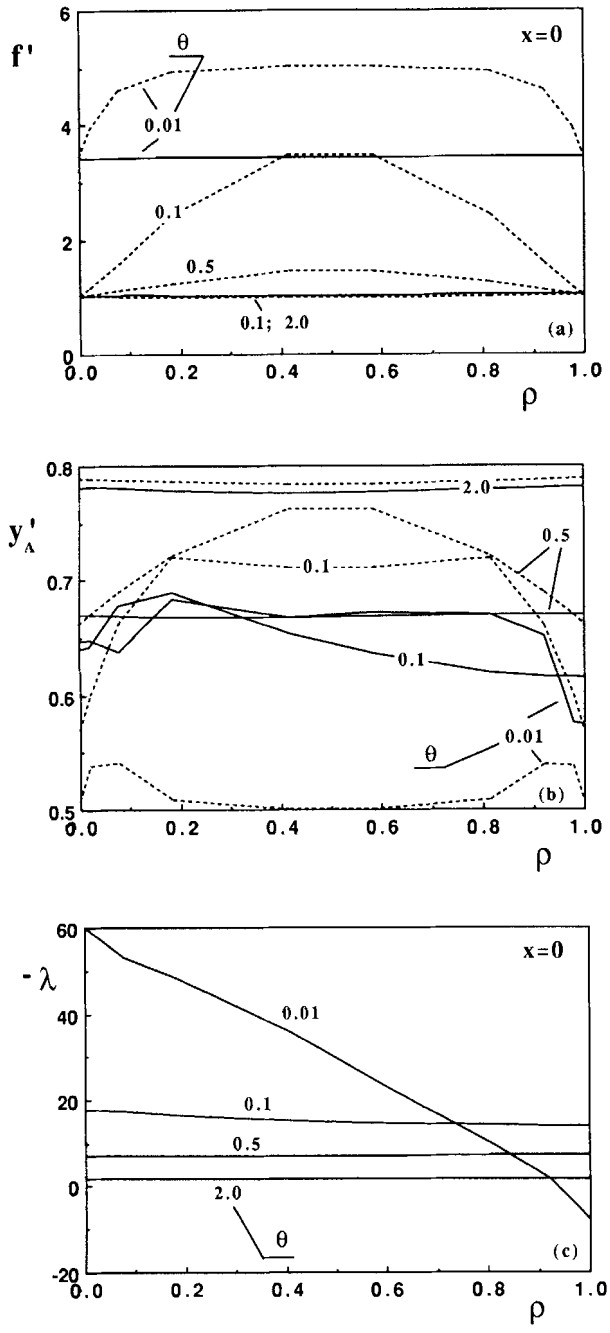

Figure 6. Intraparticle profiles of (a) reduced total pressure f', (b) mole fraction y'_A, and (c) intraparticle Peclet number λ, at the bed outlet ($x=0$) during blowdown.

$\Phi=0.2$, $m=20$, $d_p=0.1$ cm, $u_o=135$ cm/s, $\tau_o=0.446$ s; —— case A ($B_p=1.25\times10^{-9}$ cm^2), ····· case B.

Blowdown. The behavior of the system during blowdown affects the purity and recovery of a PSA process. Increasing the mass-transfer resistances inside the particles increases the depressurization time, and more adsorbable species remains in the bed at the end of blowdown ($|f_{(x=1)}-f_l|/f_l<1\%$), resulting in a lower separation.

Figures 5a-5c show the histories of reduced total pressure f at the closed end ($x=1$), mole fraction y_A and mole flux ($-u^*yA$) at the open end (bed outlet, $x=0$) as calculated by the three models with the values: $\Phi=0.2$, $m=20$, $d_p=0.1$ cm, $u_o=135$ cm/s, $\tau_o=0.446$ s, and $B_p=1.25\times10^{-9}$ cm^2 (case A). Figure 5b shows that the first mole fraction plateau at the bed outlet (Lu et al., 1991b) observed with the equilibrium model (case C, dashed lines) is smoothed out with the diffusion model (case B, dotted lines) and is somehow recovered with the diffusion/convection model (case A, solid lines). In blowdown, like in pressurization, case A is located between cases B and C, the two limiting situations.

The comments on the behavior inside the particles during pressurization are still valid during blowdown as Figures 6a-6c show: the final plateau is reached faster in case A than in case B. Moreover, Figure 6c shows that at short times the particles blow down in both directions (increasing and decreasing ρ), and the intraparticle Peclet number λ crosses the zero value; a similar situation is likely to occur also in pressurization at very short times. This happens because at short times the intraparticle pressure gradient is dominated by adsorption and desorption, not by the pressure drop across the particle. Fluxes out of both sides of the particle strongly increase at short times when the particle size increases. At long times, fluxes into and out of the particles are of the same order; however, they still increase when d_p increases. The reduced pressure profiles for the diffusion model (case B, dotted lines) in Figures 3a, 4a and 6a help understand what is happening. During adsorption, the intraparticle pressure gradients give rise to a convective flow to the center of the particle, provided that the pores are large enough; the reverse is true during desorption. In both cases, the intraparticle convective flow so generated is beneficial to the operation of the system. The importance of this intraparticle pressure gradient decreases with time in each of the steps, while the importance of the pressure drop across the particle increases, becoming dominant at larger times.

Effect of adsorbent capacity m and pressure ratio Φ

The importance of the mass-transfer rate increases with the adsorbent capacity. The larger the capacity of the adsorbent, the larger the transport of material between fluid and solid.

The final axial mole fraction profiles in pressurization for different reduced capacities m as calculated with the three models are shown in Figure 7a. The difference between the penetration distances obtained in case B (dotted lines) and in case C (dashed lines) increases with the adsorbent capacity, that is, for case B, when m increases the relative saturation of the absorbent decreases. This can be seen from Figures 8a and 8b, where the profiles of reduced pressure f' and mole fraction y'_A inside the particles, at the axial position $x=0.1$, for cases A (solid lines) and B (dotted lines) are shown based on $m=100$, $\Phi=0.2$, $d_p=0.1$ cm, $u_o=135$ cm/s, $\tau_o=0.446$ s, and $B_p=1.25\times10^{-9}$ cm^2 (case A). When the particle diameter is reduced to $d_p=0.03$ cm, the mass-transfer resistance decreases, and the diffusion model (case B) tends to, and almost coincides with, the equilibrium model (case C), as can be seen from Figure 7a.

When the pressure ratio $\Phi(\Phi=P_l/P_h)$ decreases, α increases, since both the local space time and the effective diffusivity decrease with the pressure ratio; the intraparticle convection (measured by λ) increases as well with decreasing Φ. The final

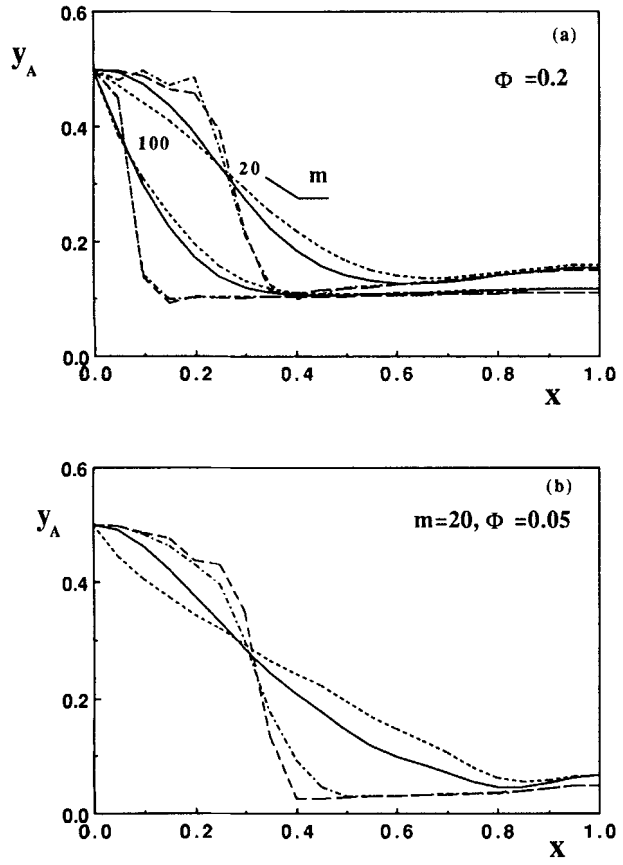

Figure 7. Influence of m and Φ on the final axial mole fraction profiles during pressurization.

(a) $\Phi = 0.2$, $d_p = 0.1$ cm, $u_o = 135$ cm/s, $\tau_o = 0.446$ s; —— case A ($B_p = 1.25 \times 10^{-9}$ cm^2), ····· case B, ------ case C, -·-·-·- case B ($d_p = 0.03$ cm, $u_o = 61.2$ cm/s, $\tau_o = 0.980$ s); (b) $\Phi = 0.05$, $m = 20$, $d_p = 0.1$ cm, $u_o = 141$ cm/s, $\tau_o = 0.425$ s; —— case A ($B_p = 2 \times 10^{-10}$ cm^2), ····· case B, ------ case C, -·-·-·- case B ($d_p = 0.03$ cm, $u_o = 7.38$ cm/s, $\tau_o = 0.813$ s).

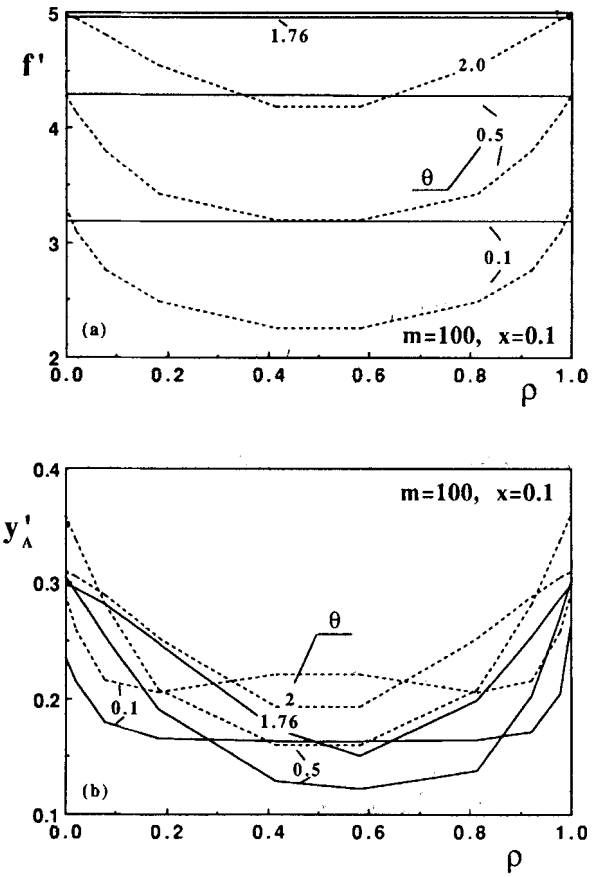

Figure 8. Intraparticle profiles of (a) reduced total pressure f' and (b) mole fraction y'_A at the axial position $x = 0.1$ in the bed.

$\Phi = 0.2$, $m = 100$, $d_p = 0.1$ cm, $u_o = 135$ cm/s, $\tau_o = 0.446$ s; —— case A ($B_p = 1.25 \times 10^{-9}$ cm^2), ····· case B.

axial mole fraction profiles for the three models are shown in Figure 7b with $m = 20$, $\Phi = 0.05$, $d_p = 0.1$ cm and 0.03 cm, and $B_p = 2 \times 10^{-10}$ cm^2 (for case A). The axial profiles of mole fraction in case B (dotted lines) are more dispersive with this lower Φ, since the mass-transfer resistance increases with α; now, even for $d_p = 0.03$ cm, a difference is observed between the profiles for cases B and C, although the diffusion model still approaches the equilibrium model when d_p is decreased. Moreover, even with a permeability six times lower, the solution of the diffusion/convection model (case A) is close to the equilibrium solution (case C) with the lower $\Phi = 0.05$ as it was with $\Phi = 0.2$: the increase of the intraparticle convective flow due to the decrease of Φ compensates for the lower permeability, improving the solution of the diffusion model (case B) as much as with higher B_p and Φ. Figures 9a and 9b show the intraparticle profiles of reduced pressure f' and mole fraction y'_A for the same case as in Figure 7b at the axial position $x = 0.25$. The increase in the intraparticle convective flow when Φ decreases is reflected on the mole fraction profiles inside the particles that become more asymmetric than with higher Φ; this comparison is shown in Figures 4b ($\Phi = 0.2$) and 9b ($\Phi = 0.05$) even with a lower permeability.

Conclusions

Pressurization and blowdown of an adsorption bed with a mixture of one inert and one adsorbable species (with uniform initial mole fraction) were studied by using three models: equilibrium, intraparticle diffusion, and intraparticle diffusion/convection.

The presence of intraparticle mass-transfer resistances increases both the pressurization and blowdown times relative to the equilibrium situation, the profiles of the adsorbable species becoming more dispersive (increasing the penetration distance) during pressurization, while at the end of blowdown the bed is less regenerated (more adsorbable species remains in the column). The results are an earlier breakthrough in the feed (production) step, which follows pressurization, and the need of a longer purge step after blowdown to regenerate the bed. The global effects are a loss in productivity, purity, and recovery.

The use of smaller particles is seldom a solution, since they lead to even higher pressurization and blowdown times (for the same productivity) with the associated mechanical problems despite the reduction of intraparticle resistances.

However, if "large-pore" materials are used in the manufacture of the adsorbent, a convective flow develops inside the

particles (near the open end of the bed where most of the mass transfer between fluid and solid occurs), enhancing the intraparticle mass-transfer rate and improving the overall behavior both in pressurization and in blowdown. The addition of intraparticle convection to a diffusion model improves the response of the bed, the limit being the equilibrium situation: the response of the diffusion/convection model is always located between two limiting situations, equilibrium and diffusion alone.

During pressurization, the intraparticle convective flow contributes up to 82.6% of the total intraparticle molar flux of species A at the bed inlet and short times $\theta = 0.01$. The improvement of the system behavior with intraparticle convection is almost independent of the capacity of the absorbent and increases when the pressure ratio $\Phi = P_l/P_h$ decreases. Linear adsorption equilibrium isotherms were assumed, because they give efficient performance in a PSA cycle; therefore, linearity of equilibrium isotherms is a target for adsorbent manufacturers. Extension to nonlinear isotherms can be found elsewhere (Lu *et al.*, 1991c).

Acknowledgment

Financial support from FUNDAÇÃO ORIENTE, JNICT, NATO CRG 890600 and EEC JOULE 0052 is gratefully acknowledged.

Notation

a_1 = parameter in Eq. 2a, g/cm^3·s
a_2 = parameter in Eq. 2a, s^2/cm^3
$b_1, \ldots, b_6$ = dimensionless constants in Table 1
B_p = permeability of the adsorbent ($\propto \bar{r}_{pore}^2$), cm^2
c = total concentration in the bulk fluid phase, mol/cm^3
c' = total concentration in the fluid inside the adsorbent, mol/cm^3
c_c = concentration in the micropores, mol/cm^3
c_o = total concentration in the bulk fluid at atmospheric pressure, mol/cm^3
c_f = feed total concentration, mol/cm^3
d_c = crystal diameter, cm
d_p = adsorbent particle diameter, cm
D_{ax} = axial dispersion coefficient, cm^2/s
D_{eA} = effective diffusivity of species A, cm^2/s
D_{mo} = molecular diffusivity at atmospheric pressure, cm^2/s
D_{kA} = Knudsen diffusivity of species A, cm^2/s
f = dimensionless total concentration in the bulk fluid phase
f' = dimensionless total concentration in the fluid inside the particle
f_h = dimensionless total concentration at high pressure
f_l = dimensionless total concentration at low pressure
f_o = dimensionless total initial concentration in the fluid
L = bed length, cm
ℓ = slab thickness, cm
m = slope of the linear adsorption equilibrium isotherm
N = dimensionless total mole flux from the bulk fluid to the adsorbent
N_A = dimensionless mole flux of species A from the bulk fluid to the adsorbent
P = pressure in the bulk fluid, Pa
P' = pressure in the fluid inside particle, Pa
Pe = Peclet number ($=uL/D_{ax}$), dimensionless
P_h = high pressure, Pa
P_l = low pressure, Pa
P_o = atmospheric pressure, Pa
ΔP_o = reference pressure drop across the bed under steady state, Pa
$\bar{r}_{pore}$ = average macropore radius, cm
t = time, s
u = superficial velocity in the bulk fluid, cm/s

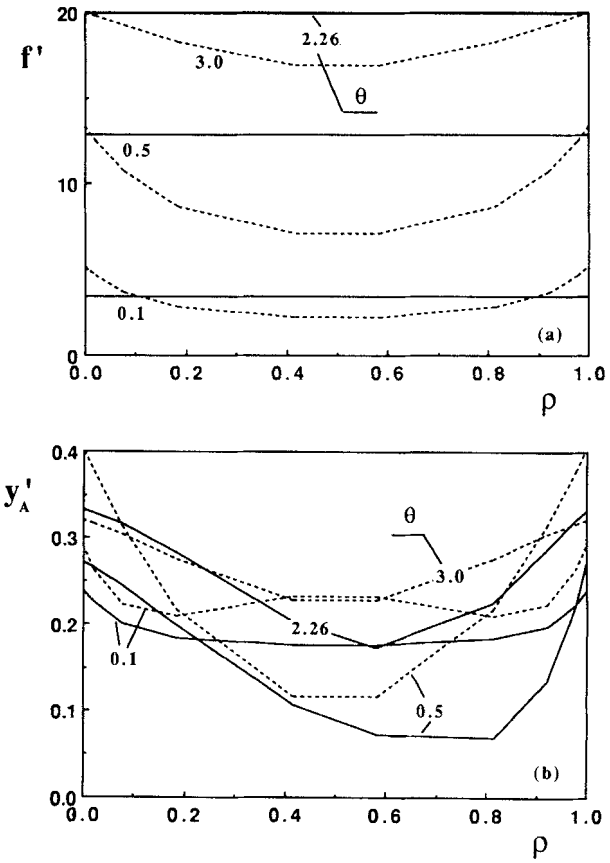

Figure 9. Intraparticle profiles of (a) reduced total pressure f' and (b) mole fraction y'_A at the axial position $x = 0.25$ in the bed.

$\Phi = 0.05$, $m = 20$, $d_p = 0.1$ cm, $u_o = 141$ cm/s, $\tau_o = 0.425$ s; —— case A ($B_p = 2 \times 10^{-10}$ cm^2), ····· case B.

u^* = dimensionless velocity in the bulk fluid
u_o = superficial velocity at the bed inlet under steady state, cm/s
v = intraparticle velocity, cm/s
v^* = dimensionless intraparticle velocity
v_o = reference intraparticle velocity, cm/s
x = dimensionless axial coordinate in the bed
y_A = mole fraction of species A in the bed
y_f = mole fraction of species A in the feed
y'_A = mole fraction of species A in the fluid inside the adsorbent
y_o = mole fraction of species A initially in the bed
z = axial coordinate in the bed, cm
z' = space coordinate in the adsorbent, cm

Greek letters

α = ratio between the time constant for intraparticle diffusion and space time, Table 1
α_o = reference parameter, Table 1
β_l = constant defined in Table 1
β_R = ratio between the half thickness of the slab and bed length, Table 1
ϵ = bed porosity
ϵ_p = adsorbent porosity
Φ = pressure ratio $\Phi = P_l/P_h$
λ = intraparticle Peclet number, Table 1
λ_o = intraparticle Peclet number at reference conditions, Table 1
μ = fluid viscosity, g/cm·s
ρ = dimensionless space coordinate in the adsorbent

ρ_o = fluid density, g/cm^3
θ = time reduced by the reference space time
γ_1, γ_2 = constants (coefficients in the axial dispersion correlation)
τ_f = tortuosity factor for the particle
τ_o = reference space time, s
ξ_p = adsorbent capacity factor

Literature Cited

Bird, R. B., W. E. Stewart, and E. N. Lightfoot, *Transport Phenomena*, pp. 150, 200, Wiley, New York (1960).

Buzanowski, W. A., R. T. Yang, and O. W. Hass, "Direct Observation of the Effects of Bed Pressure Drop on Adsorption and Desorption Dynamics," *Chem. Eng. Sci.*, **44**, 2392 (1989).

Cheng, H. C., and F. B. Hill, "Separation of Helium-Methane Mixtures by Pressure Swing Adsorption," *AIChE J.*, **31**, 95 (1985).

Doong, S. J., and R. T. Yang, "Bulk Separation of Multicomponent Gas Mixture by Pressure Swing Adsorption: Pore/Surface Diffusion and Equilibrium Models," *AIChE J.*, **32**, 397 (1986).

Doong, S. J., and R. T. Yang, "The Role of Pressure Drop in Pressure Swing Adsorption," *AIChE Symp. Ser.*, **45**(84), 264 (1988).

Farooq, S. D., D. M. Ruthven, and H. A. Boniface," Numerical Simulation of a Pressure Swing Adsorption Oxygen Unit," *Chem. Eng. Sci.*, **44**, 2809 (1989).

Farooq, S. D., and D. M. Ruthven, "Numerical Simulation of a Kinetically Controlled Pressure Swing Adsorption Bulk Separation Process Based on a Diffusion Model," *Chem. Eng. Sci.*, **46**, 2213 (1991).

Fernandez, G. F., and C. N. Kenney, "Modeling of the Pressure Swing Air Separation Processes," *Chem. Eng. Sci.*, **38**, 827 (1983).

Hart, J., M. Battrum, and W. J. Thomas, "Axial Pressure Gradients During Pressurization and Depressurization Steps of a PSA Gas Separation Cycle," *Gas Sep. and Purif.*, **4**, 97 (1990).

Hassan, M. M., N. S. Raghavan, and D. M. Ruthven, "Air Separation by Pressure Swing Adsorption on a Carbon Molecular Sieve," *Chem. Eng. Sci.*, **41**, 1333 (1986).

Hassan, M. M., N. S. Raghavan, and D. M. Ruthven, "Pressure Swing Adsorption Air Separation on a Carbon Molecular Sieve: II," *Chem. Eng. Sci.*, **42**, 2037 (1987).

Jones, R. L., G. E. Keller, and R. C. Wells, "Rapid Pressure Swing Adsorption Process with High Enrichment Factor," *U.S. Patent 4,194,892* (1980).

Jones, R. L., and G. E. Keller, "Pressure Swing Parametric Pumping—a New Adsorption Process," *J. Sep. Proc. Technol.*, **2**, 17 (1981).

Leitão, A., and A. E. Rodrigues, "Fixed-Bed Reactor for Gasoline Sweetening: Kinetics of Mercaptan Oxidation and Simulation of the Merox Reactor Unit," *Chem. Eng. Sci.*, **45**, 679 (1990).

Lu, Z. P., J. M. Loureiro, M. D. LeVan, and A. E. Rodrigues, "Effect of Intraparticle Forced Convection on Gas Desorption from Fixed-Bed Containing 'Large-Pore' Adsorbents," *Ind. Eng. Chem. Res.*, in press (1991a).

Lu, Z. P., J. M. Loureiro, M. D. LeVan, and A. E. Rodrigues, "Pressurization of Adsorption Beds: II. Effect of the Momentum and Equilibrium Relations on the Isothermal Operation," *Chem. Eng. Sci.*, submitted (1991b).

Lu, Z. P., J. M. Loureiro, M. D. LeVan, and A. E. Rodrigues, Intraparticle Diffusion/Convection Models in Pressurization and Blowdown: Nonlinear Equilibrium," AIChE Meeting, Los Angeles; *Sep. Sci. Technol.*, accepted (1991c).

Richter, E., J. Strunk, K. Knoblauch, and H. Juntgen, "Modeling of Desorption by Depressurization as Partial Step in Gas Separation by Pressure Swing Adsorption," *Ger. Chem. Eng.*, **5**, 147 (1982).

Rodrigues, A. E., B. Ahn, and A. Zoulalian, "Intraparticle Forced Convection Effect in Catalyst Diffusivity Measurements and Reactor Design," *AIChE J.*, **28**, 541 (1982).

Rodrigues, A. E., Z. P. Lu, and J. M. Loureiro, "Residence Time Distribution of Inert and Linearly Adsorbed Species in Fixed-Bed Containing 'Large-Pore' Supports: Applications in Separation Engineering," *Chem. Eng. Sci.*, **46**, 2765 (1991a).

Rodrigues, A. E., J. M. Loureiro, and M. D. LeVan, "Simulated Pressurization of Adsorption Beds," *Gas Sep. and Purif.*, **5**, 115 (1991b).

Rodrigues, A. E., Z. P. Lu, J. M. Loureiro, and M. D. LeVan, "Pressurization of Adsorption Beds," NSF-CNRS Workshop on Adsorption Processes for Gas Separation, Gif-sur-Yvette, France (1991c).

Rodrigues, A. E., J. C. Lopes, Z. P. Lu, J. M. Loureiro, and M. M. Dias, "Importance of Intraparticle Convection on the Performance of Chromatographic Processes," *Int. Symp. Prep. Chromat.*, Arlington, VA (1991); *J. Chromatogr.*, **590**, 93 (1992).

Rota, R., and P. C. Wankat, "Intensification of Pressure Swing Adsorption Processes," *AIChE J.*, **36**, 1299 (1990).

Ruckenstein, E., A. Vaidyanathan, and G. R. Youngquist, "Sorption by Solids with Bidisperse Pore Structures," *Chem. Eng. Sci.*, **26**, 1306 (1971).

Ruthven, D. M., and K. F. Loughlin, "The Diffusional Resistance of Molecular Sieve Pellets," *Can. J. Chem. Eng.*, **50**, 550 (1972).

Ruthven, D. M., "Sorption Kinetics in PSA Systems," *Symp. on Gas Separation by PSA*, Twente University, Netherlands (Feb. 1992).

Shin, H. S., and K. S. Knaebel, "Pressure Swing Adsorption: a Theoretical Study of Diffusion-Induced Separation," *AIChE J.*, **33**, 654 (1987).

Shin, H. S., and K. S. Knaebel, "Pressure Swing Adsorption: an Experimental Study of Diffusion-Induced Separation," *AIChE J.*, **34**, 1409 (1988).

Skarstrom, C. W., "Use of Adsorption Phenomena in Automatic Plant-Type Gas Analyzers," *New York Acad. Sci.*, **72**, 751 (1959).

Sundaram, N., and P. Wankat, "Pressure Drop Effects in the Pressurization and Blowdown Steps of Pressure Swing Adsorption," *Chem. Eng. Sci.*, **43**, 123 (1988).

Wankat, P. C., "Intensification of Sorption Processes," *Ind. Eng. Chem. Res.*, **26**, 1579 (1987).

Wankat, P. C., and Y. M. Koo, "Scaling Rules for Isocratic Elution Chromatography," *AIChE J.*, **34**, 1006 (1988).

Yang, R. T., *Gas Separation by Adsorption Processes*, Butterworths, Boston (1987).

Yang, R. T., and S. J. Doong, "Gas Separation by Pressure Swing Adsorption: a Pore-Diffusion Model for Bulk Separation," *AIChE J.*, **31**, 1829 (1985).

Yang, R. T., S. J. Doong, and P. L. Cen, "Bulk Gas Separation of Binary and Ternary Mixtures by Pressure Swing Adsorption," *AIChE Symp. Ser.*, **81**(242), 84 (1985).

Zhong, G. M., F. Meunier, S. Huberson, and J. B. Chalfen, "Pressurization of a Single Component Gas in an Adsorption Column," *Chem. Eng. Sci.*, **47**, 543 (1992).

Manuscript received Nov. 4, 1991, and revision received Mar. 23, 1992.